ELSEVIER

Nuclear Instruments and Methods in Physics Research A 398 (1997) 109–125

NUCLEAR INSTRUMENTS & METHODS IN PHYSICS RESEARCH Section A

A line-shape analysis for spin-1 NMR signals

The Spin Muon Collaboration (SMC)

C. Dulya[a,b,*], D. Adams[c], B. Adeva[d], E. Arik[e], A. Arvidson[f], B. Badelek[f,g], M.K. Ballintijn[b,1], D. Bardin[2], G. Bardin[h], G. Baum[i], P. Berglund[j], L. Betev[k], I.G. Bird[h,3], R. Birsa[l], P. Björkholm[f], B.E. Bonner[c], N. de Botton[h], M. Boutemeur[m,4], F. Bradamante[l,5], A. Bressan[l,6], S. Bültmann[i,7], E. Burtin[h], C. Cavata[h], D. Crabb[n], J. Cranshaw[c,8], T. Çuhadar[e], S. Dalla Torre[l], R. van Dantzig[b], B. Derro[a], A. Deshpande[m], S. Dhawan[m], A. Dyring[f], S. Eichblatt[c,9], J.C. Faivre[h], D. Fasching[o,10], F. Feinstein[h], C. Fernandez[d,p], B. Frois[q,h], A. Gallas[d], J.A. Garzon[d,p], T. Gaussiran[c], R. Gehring[r], M. Giorgi[l], E. von Goeler[s], St. Goertz[r], F. Gomez[d], G. Gracia[d], N. de Groot[b,11], M. Grosse Perdekamp[a,12], E. Gülmez[c], J. Harmsen[r], D. von Harrach[t], T. Hasegawa[u,13], P. Hautle[q,14], N. Hayashi[u,15], C.A. Heusch[q,16], N. Horikawa[u], V.W. Hughes[m], G. Igo[a], S. Ishimoto[u,17], T. Iwata[v], E.M. Kabuß[t], T. Kageya[u], L. Kalinovskaya[w,18], A. Karev[w], H.J. Kessler[x], T.J. Ketel[b], A. Kishi[v], Yu. Kisselev[w], L. Klostermann[b,19], D. Krämer[i], V. Krivokhijine[w], W. Kröger[q,16], V. Kukhtin[w], K. Kurek[g], J. Kyynäräinen[q,j], M. Lamanna[l], U. Landgraf[x], J.M. Le Goff[h,q], F. Lehar[h], A. de Lesquen[h], J. Lichtenstadt[y], T. Lindqvist[f], M. Litmaath[b,5], M. Lowe[c,10], A. Magnon[h], G.K. Mallot[t], F. Marie[h], A. Martin[l], J. Martino[h], T. Matsuda[u,13], B. Mayes[p], J.S. McCarthy[h], K. Medved[w], W. Meyer[r], G. van Middelkoop[b], D. Miller[o], K. Mori[z], J. Moromisato[s], A. Nagaitsev[w],

* Corresponding author. E-mail: chris.dulya@ciemat.es.

[1] Now at Pure Atria, Hoofddorp, The Netherlands.

[2] Permanent address: Institut für Hochenergiephysik, Platanenallee 6 D-15738 Zeuthen, Germany.

[3] Now at Institut de Physique Nucléaire, Université de Lausanne, 1015 Lausanne, Switzerland.

[4] Now at University of Montreal, PQ, H3C 3J7, Montreal, Canada.

[5] Now at CERN, 1211 Geneva 23, Switzerland.

[6] Now at DPhNC, University of Geneva, Geneva, Switzerland.

[7] Now at University of Virginia, Department of Physics, Charlottesville, 22901 VA, USA[31].

[8] Now at INFN Trieste, 34127 Trieste, Italy.

[9] Now at Fermi National Accelerator Laboratory, Batavia, 60510 IL, USA.

[10] Now at University of Wisconsin, USA.

[11] Now at SLAC, Stanford, 94309 CA, USA.

[12] Now at Yale University, Department of Physics, New Haven, 06511 CT, USA[31].

[13] Permanent address: Miyazaki University, Faculty of Engineering, 889-21 Miyazaki-Shi, Japan.

[14] Permanent address: Paul Scherrer Institut, 5232 Villigen, Switzerland.

[15] Permanent address: The Institute of Physical and Chemical Research (RIKEN), wako 351-01, Japan.

[16] Permanent address: University of California, Institute of Particle Physics, Santa Cruz, 95064 CA, USA.

[17] Permanent address: KEK, Tsukuba-Shi, 305 Ibaraki-Ken, Japan.

[18] Permanent address: Bogoliubov Laboratory for Theoretical Physics, JINR, ul. Joliot-Curie 6 RU-141980 Dubna, Russia.

PII S0168-9002(97)00317-3

J. Nassalski[g], L. Naumann[q, 20], T.O. Niinikoski[q], J.E.J. Oberski[b], A. Ogawa[v], C. Ozben[e], D.P. Parks[p], F. Perrot-Kunne[h], D. Peshekhonov[w], R. Piegaia[m, 21], L. Pinsky[p], S. Platchkov[h], M. Plo[d], D. Pose[w], H. Postma[b], J. Pretz[t], T. Pussieux[h], J. Pyrlik[p], G. Reicherz[r], I. Reyhancan[e], A. Rijllart[q], J.B. Roberts[c], S. Rock[q, 22], M. Rodriguez[d, 23], E. Rondio[g], A. Rosado[k], I. Sabo[m], J. Saborido[d], A. Sandacz[g], I. Savin[w], P. Schiavon[l], K.P. Schüler[m, 24], R. Segel[o], R. Seitz[t, 25], Y. Semertzidis[q, 8], F. Sever[b, 26], P. Shanahan[o, 9], E.P. Sichtermann[b], F. Simeoni[l], G.I. Smirnov[w], A. Staude[k], A. Steinmetz[t], U. Stiegler[q], H. Stuhrmann[aa], M. Szleper[g], K.M. Teichert[k], F. Tessarotto[l], W. Tlaczala[g, 27], A. Tripet[k, b], G. Unel[a], M. Velasco[o, 5], J. Vogt[k], R. Voss[q], R. Weinstein[p], C. Whitten[a], R. Windmolders[ab], R. Willumeit[aa], W. Wislicki[g], A. Witzmann[x], A. Yañez[d], J. Ylöstalo[j], A.M. Zanetti[l, 28], K. Zaremba[g], J. Zhao[aa]

[a] *University of California, Department of Physics, Los Angeles, 90024 CA, USA*[31]

[b] *NIKHEF, Delft University of Technology, FOM and Free University, 1009 AJ Amsterdam, The Netherlands*[34]

[c] *Rice University, Bonner Laboratory, Houston, 77251-1892 TX, USA*[31]

[d] *University of Santiago, Department of Particle Physics, 15706 Santiago de Compostela, Spain*[36]

[e] *Bogaziçi University and Çekmece Nuclear Research Center, Istanbul Technical University, Istanbul University, Istanbul, Turkey*[30]

[f] *Uppsala University, Department of Radiation Sciences, 75121 Uppsala, Sweden*

[g] *Soltan Institute for Nuclear Studies and Warsaw University, 00681 Warsaw, Poland*[38]

[h] *DAPNIA, C.E. Saclay, 91191 Gif-sur-Yvette, France*[35]

[i] *University of Bielefeld, Physics Department, 33501 Bielefeld, Germany*[29]

[j] *Helsinki University of Technology, Low Temperature Laboratory and Institute of Particle Physics Technology, Otakaari 3A, 02150 Finland*

[k] *University of Munich, Physics Department, 80799 Munich, Germany*[29]

[l] *INFN Trieste and University of Trieste, Department of Physics, 34127 Trieste, Italy*

[m] *Yale University, Department of Physics, New Haven, 06511 CT, USA*[31]

[n] *University of Virginia, Department of Physics, Charlottesville, 22901 VA, USA*[31]

[o] *Northwestern University, Department of Physics, Evanston, 60208 IL, USA*[31,32]

[p] *University of Houston, Department of Physics, Houston, 77204-5504 TX, and Institute for Beam Particle Dynamics, Houston, 77204-5506 TX, USA*[31,32]

[q] *CERN, 1211 Geneva 23, Switzerland*

[19] Now at Ericsson Telecommunication, 5120 AA Rijen, The Netherlands.

[20] Deceased.

[21] Permanent address: University of Buenos Aires, Physics Department, 1428 Buenos Aires, Argentina.

[22] Permanent address: The American University, Washington D.C. 20016, USA.

[23] Now at Uppsala University, 75121 Uppsala, Sweden.

[24] Now at DESY.

[25] Now at Dresden Technical University, 01062 Dresden, Germany
Permanent address: Brookhaven National Laboratory, Upton, 11973 NY, USA.

[26] Present address: ESFR, F-38043 Grenoble, France.

[27] Now at Institute of Physics, Warsaw University of Technology.

[28] Now at Institute of Radioelectronics, Warsaw University of Technology.

[29] Supported by the Bundesministerium für Bildung, Wissenschaft, Forschung und Technologie.

[30] Partially supported by TUBITAK and the Centre for Turkish-Balkan Physics Research and Application (Bogaziçi University).

[31] Supported by the U.S. Department of Energy.

[32] Supported by the U.S. National Science Foundation.

[33] Supported by Ishida Foundation, Monbusho Grant-in-Aid for Scientific Research (International Scientific Research Program and Specially Promoted Research).

[34] Supported by the National Science Foundation (NWO) of the Netherlands.

[35] Supported by the Commissariat à l'Energie Atomique.

[36] Supported by Comision Interministerial de Ciencia y Tecnologia.

[37] Supported by the Israel Science Foundation.

[38] Supported by KBN SPUB/P3/209/94.

[r] University of Bochum, Physics Department, 44780 Bochum, Germany[29]
[s] Northeastern University, Department of Physics, Boston, 02115 MA, USA[32]
[t] University of Mainz, Institute for Nuclear Physics, 55099 Mainz, Germany[29]
[u] Nagoya University, CIRSE, Furo-Cho, Chikusa-Ku, 464 Nagoya, Japan[33]
[v] Nagoya University, Department of Physics, Furo-Cho, Chikusa-Ku, 464 Nagoya, Japan[33]
[w] JINR, Laboratory of Particle Physics, Dubna, Russia
[x] University of Freiburg, Physics Department, 79104 Freiburg, Germany[29]
[y] Tel Aviv University, School of Physics, 69978 Tel Aviv, Israel[37]
[z] Nagoya University, College of Medical Technology, Daikominami 1, Higashi-Ku, 461 Nagoya, Japan[33]
[aa] GKSS, 21494 Geesthacht, Germany[29]
[ab] University of Mons, Faculty of Science, 7000 Mons, Belgium

Received 5 December 1996

Abstract

An analytic model of the deuteron absorption function has been developed and is compared to experimental NMR signals of deuterated butanol obtained at the SMC experiment in order to determine the deuteron polarization. The absorption function model includes dipolar broadening and a frequency-dependent treatment of the intensity factors. The high-precision TE signal data available are used to adjust the model for Q-meter distortions and dispersion effects. Once the Q-meter adjustment is made, the enhanced polarizations determined by the asymmetry and TE-calibration methods compare well within the accuracy of each method. In analyzing the NMR signals, the quadrupolar coupling constants could be determined for both the C–D and the O–D bonds of deuterated butanol.

1. Introduction

Two methods to measure deuteron polarization will be compared in this paper. The "area" method uses the ratio of enhanced and thermal equilibrium (TE) signals to determine the polarization (labeled P_{AR}) in a manner which is mostly insensitive to distortions caused by the electronics of the NMR system. However, it is noise limited due to the small size of the TE signals. The "asymmetry" method fits a theoretical model of the deuteron absorption function to NMR signal data determining the polarization (labeled P_{AS}) from the shape of the signal. The absorption function presented in this paper assumes that the spin temperature of the system is uniform throughout the sampling range of the NMR coils. Frequency-dependent distortions caused by the NMR system influence the value of the polarization measured by the asymmetry method. However, TE-signals can be used to determine the instrument effects and then the polarization values calculated with the asymmetry method and the thermal equilibrium method agree within the accuracies of each method. In addition, using the theoretical absorption function developed here, the values of the electric quadrupolar coupling constants in the C–D and the O–D bonds of deuterated butanol (C_4D_9OD) were able to be determined.

1.1. Nuclear susceptibility and polarization

Consider a system of particles with spin each having a magnetic moment $\boldsymbol{\mu}$ in a magnetic field $\boldsymbol{H}_0$. There will be a Zeeman energy splitting of a spin-I system into $2I + 1$ levels separated in energy by $\hbar\omega_0 = -\boldsymbol{\mu} \cdot \boldsymbol{H}_0/I = g\mu_N H_0$, where g is the g-factor of the particle with spin and μ_N is the nuclear magneton.

When the spin system is irradiated by radio frequency (RF) energy at the Larmor frequency the spins either absorb some energy or the RF induces the spins to emit energy. The response of a spin system to RF irradiation is described by its magnetic susceptibility $\chi(\omega) = \chi'(\omega) - i\chi''(\omega)$ in which χ'' is the absorption function and χ' is the dispersion function. The static susceptibility is $\chi_0 = \chi(0) = \chi'(0)$. The deuteron absorption function whose maximum occurs at its Larmor frequency ω_d only extends over about a $2\pi \times 300\,\text{kHz}$ range, outside of which the dispersion function can be considered to have constant value χ_0. The spin polarization of the

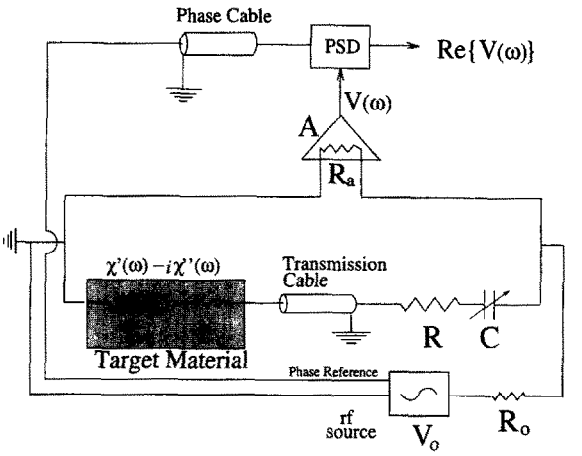

Fig. 1. A block diagram of the Q-meter circuit detecting the real part of the NMR signal.

material is given by the integral of the absorption function [1]

$$P = \left(\frac{2\hbar I}{g^2\mu_N^2\pi N}\right)\int_0^\infty \frac{\omega_d\chi''(\omega)}{\omega}\,d\omega, \tag{1}$$

where N is the number of spins. The general characteristics of the absorption function for deuterated butanol can be seen in Figs. 6 and 7, and are discussed in more detail later in Section 2 of this paper.

1.2. Detection of the deuteron absorption function

In order to measure the absorption function, a coil of inductance L_c and resistance r_c is embedded in the target material. Through the inductive coupling between the spins and the coil, the impedance of the coil will become [2]

$$Z_c = r_c + i\omega L_c(1 + 4\pi\eta\chi(\omega)), \tag{2}$$

where η is the filling factor of the coil. The change of impedance is detected by a continuous-wave constant current Q-meter [3] connected to a series LRC resonant circuit as shown in Fig. 1. Here, the LRC circuit consists of the NMR coil connected via a coaxial transmission line to the damping resistor, R, and the tuning capacitor, C. A frequency synthesizer connected to the Q-meter sweeps the RF frequency ω over values where χ'' is nonzero. A complex voltage $V = V(\omega,\chi)$ which is a function of Z_c, and hence of χ, is generated if the current is constant. The voltage is a superposition of both the signal proportional to χ and the so-called Q-curve, which is the response of the Q-meter to ω in the absence of χ. The last stage of the Q-meter selects the real part of the voltage by using the input RF signal as a reference. The Q-curve is made symmetric around ω_d by adjusting the capacitance C. The Q-curve is measured separately by changing H_0 such that ω_d is well outside the range of the frequency scan of the Q-meter in which case χ'' vanishes and χ' is negligible. The two signals are subtracted and the result is the NMR signal

$$S(\omega) = \mathrm{Re}\{V(\omega,\chi) - V(\omega,0)\} \propto \chi''(\omega)\ . \tag{3}$$

In a magnetic field of 2.5 T, the deuteron Larmor frequency is $2\pi \times 16.35$ MHz. Thus, the polarization for deuterons can be approximated by

$$P = \mathscr{K}\int \frac{\omega_d S(\omega)}{\omega}\,d\omega, \tag{4}$$

where the integration limits (sweeping range of the Q-meter) extend over a $2\pi \times 500$ kHz band around the Larmor frequency which is the full range where χ'' is nonzero. The constant $\mathscr{K}$ contains all the unknown

frequency-independent gains in the Q-meter and is determined by making a thermal equilibrium (TE) calibration [4] of the system. In a TE calibration, NMR signals are taken at a temperature around 1 K with the spin system in thermal equilibrium with the lattice. The polarization calculated from the spin-1 Brillouin function is

$$P = \frac{4\tanh(\hbar\omega_d/2kT)}{3+\tanh^2(\hbar\omega_d/2kT)} \approx \frac{4}{3}\tanh(\hbar\omega_d/2kT), \tag{5}$$

where k is Boltzmann's constant and T is the temperature. For $\omega_d = 2\pi \times 16.35\,\text{MHz}$ and $T = 1\,\text{K}$, the polarization is $P = 0.0523\,\%$ at TE for deuterons. Thus, the TE calibration determines the constant $\mathscr{K}$ in the following manner:

$$\mathscr{K} = \frac{4\tanh(\hbar\omega_d/2kT)}{3\int d\omega\ \omega_d S(\omega)/\omega}. \tag{6}$$

The small polarization of the TE signals limits resolution of measuring $\mathscr{K}$ by Eq. (6) because the noise on the signal is appreciable. Normally, one TE signal is the average of 2000 or so double sweeps [5] over the 500 kHz sweep range. However, the noise on a TE signal is large even if 2000 sweeps are used. By taking many signals and measuring the temperature for each signal, an average constant $\mathscr{K}$ is determined. The averaging significantly reduces the noise as can be seen in Fig. 2, where 380 TE signals of 2000 double sweeps are averaged, resulting in a "super-TE-signal."

After the calibration constant $\mathscr{K}$ has been measured, Eq. (4) can be used to determine the polarization of the material in the enhanced polarization state once the integral of the NMR signal is determined. Enhanced polarization is attained via the dynamic nuclear polarization (DNP) process [6] in which microwaves are used to increase the polarization. Enhanced polarizations of $P \gtrsim \pm 50\%$ are obtainable [4,7] for deuterons, and they produce much larger signals than TE polarizations. Thus, only 200 double sweeps are needed for sufficient noise reduction to allow an accurate area determination of an enhanced signal.

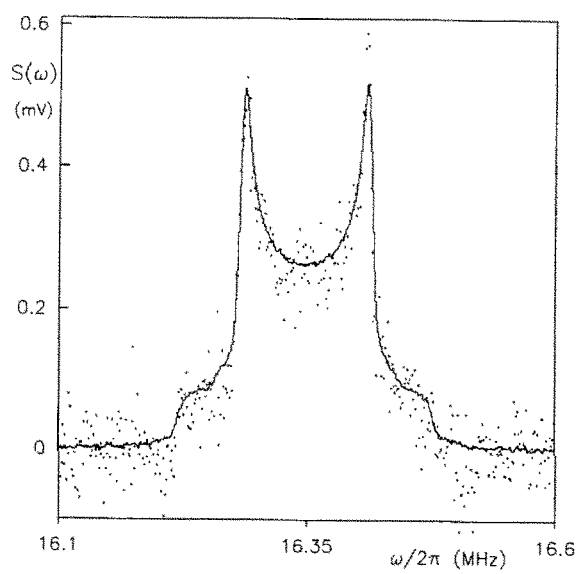

Fig. 2. A TE signal and a super-TE-signal. The dots are the data points of a 2000 double sweep TE signal. The line is a super-TE-signal which is the average of 380 TE signals, which means 760 000 double sweeps in total. The averaging reduces the noise sufficiently to allow a determination of the calibration constant $\mathscr{K}$, and in addition, reliable fitting.

2. Quadrupole resonance lines

At this point, the theoretical model for the line shape of the absorption function for deuterated butanol (C_4D_9OD) needs to be developed. In the model, first-order quadrupole splitting with electric field gradients which can be asymmetric about the bond axes is considered.

The Zeeman splitting of a spin-1 system in a magnetic field has three evenly spaced quantized energy levels. However, in deuterated butanol, as in many other materials which do not have cubic symmetry, there are local electric field gradients that couple to the quadrupole moments of the deuterons causing an asymmetric splitting of the energy levels into two overlapping absorption lines. In the case of deuterated butanol, the C–D and the O–D bonds generate the fields. The quadrupole tensor ($\overleftrightarrow{Q}$) of the deuteron couples to the gradient of the electric field ($\nabla \boldsymbol{E}$) [8] arising from the atomic electrons in the bonds. The energy levels of such a spin-1 system are written as [9–11]

$$E_m = -\hbar\omega_d m + \hbar\omega_q\{3\cos^2(\theta) - 1 + \eta\sin^2(\theta)\cos(2\phi)\}(3m^2 - 2), \tag{7}$$

where θ is the polar angle between the axis given by the C–D or O–D bond and the magnetic field $\boldsymbol{H}_0$, and $m = -1, 0, 1$ is the spin magnetic quantum number. An often used notation for the quadrupole interaction is $\hbar\omega_q = \mathrm{eq}\,\mathrm{eQ}/8$, where eq is the magnitude of the electric field gradient along the bond direction and eQ is the electric quadrupole moment of the deuteron. The azimuthal angle ϕ and parameter η are necessary for describing bonds where the electric field gradient is not symmetric about the bond axis. Specific definitions of eq, eQ, η, and ϕ can be found in Refs. [12,13]. The electric field gradient has different values for the two types of bonds, while the quadrupole moment is of course the same.

For a given value of θ, there are two resonant frequencies in this system which correspond to the positive $E_0 \leftrightarrow E_1$ transition with energy $\Delta E_+ = E_0 - E_1$ and intensity I_+ and the negative $E_{-1} \leftrightarrow E_0$ transition with energy $\Delta E_- = E_{-1} - E_0$ and intensity I_-. These two resonant frequencies are

$$\Delta E_\pm \overset{\text{def}}{=} \hbar\omega_\pm = \hbar\omega_d \mp 3\hbar\omega_q\{[3 - \eta\cos(2\phi)]\cos^2(\theta) - [1 - \eta\cos(2\phi)]\}, \tag{8}$$

which are no longer equal as in the case of pure Zeeman splitting. However, in practice, a single RF frequency ω is applied to the material which stimulates one of the two transitions depending on θ, that is, the orientation of the bond. Solving Eq. (8) for θ, we have

$$\cos(\theta_\varepsilon) = \sqrt{\frac{1 - \varepsilon R - \eta\cos(2\phi)}{3 - \eta\cos(2\phi)}}, \tag{9}$$

where the subscript $\varepsilon = \pm 1$ is attached to the angle instead of the frequency and the dimensionless variable $R = (\omega - \omega_d)/3\omega_q$ is used as a shorthand notation. In other words, RF irradiation of a frequency ω induces the $I_\pm$ transition for bonds having an angle $\theta_\pm$. Since $0 \le \cos^2(\theta) \le 1$, the allowed ranges of ω are

$$-2 < R < [1 - \eta\cos(2\phi)] \tag{10}$$

for the I_+ transition and

$$-[1 - \eta\cos(2\phi)] < R < 2 \tag{11}$$

for the I_- transition. Thus, the absorption function spans a range from $-2 < R < 2$ with the peaks occurring at $R = \pm[1 - \eta\cos(2\phi)]$. The intensities $I_\pm$ reflect the net number of spins available for making a particular transition. The absorption function line shape as a function of frequency for an even distribution of the solid angle (random orientation of the molecules) can be split into

$$\chi''(\omega) \sim \sum_{\varepsilon=\pm 1}\left|\frac{\mathrm{d}I_\varepsilon(\theta)}{\mathrm{d}\omega}\right| = \sum_{\varepsilon=\pm 1}\left|\frac{\mathrm{d}I_\varepsilon(\theta)}{\mathrm{d}(\cos\theta_\varepsilon)}\frac{\mathrm{d}(\cos\theta_\varepsilon)}{\mathrm{d}\omega}\right|$$

$$\sim \sum_{\varepsilon=\pm 1} \left| \frac{\mathrm{d}I_\varepsilon(\theta)}{\mathrm{d}(\cos\theta_\varepsilon)} \times \frac{1}{\omega_\mathrm{q}} \frac{\sqrt{3}}{\sqrt{3-\eta\cos(2\phi)}} \frac{\varepsilon}{\sqrt{1-\varepsilon R-\eta\cos(2\phi)}} \right| . \tag{12}$$

The angular dependence of the intensity factors $(\mathrm{d}I_\varepsilon(\theta)/\mathrm{d}(\cos\theta_\varepsilon))$ will be elaborated in the next section so that the dipolar broadening of the density of states $(\mathrm{d}(\cos\theta_\varepsilon)/\mathrm{d}\omega)$ can be considered next.

The interaction of deuterons with surrounding deuterons and other spins leads to a dipolar broadening of the spectrum. Spin–spin interactions cause the local field at a given spin to be distributed about H_0, thus ω_d varies slightly for each spin. So, in order to refine the model in Eq. (12), the dipolar broadening of the density of states is taken into account. If the distribution of ω_d is assumed to be Lorentzian, the resulting intensity spectrum is a convolution of the density of states with a Lorentzian function

$$\begin{aligned} f_\varepsilon(R,A,\eta,\phi) &= \int_{-2\varepsilon}^{\varepsilon[1-\eta\cos(2\phi)]} \frac{1}{\sqrt{1-\varepsilon x-\eta\cos(2\phi)}} \frac{A/\pi}{A^2+\varepsilon^2(x-R)^2}\,\mathrm{d}(\varepsilon x) \\ &= \frac{2A}{\pi}\int_0^Y \frac{\mathrm{d}y}{y^4-2[1-\varepsilon R-\eta\cos(2\phi)]y^2+A^2+[1-\varepsilon R-\eta\cos(2\phi)]^2}, \end{aligned} \tag{13}$$

where substitutions $y=\sqrt{1-\varepsilon x-\eta\cos(2\phi)}$ and $Y=\sqrt{3-\eta\cos(2\phi)}$ for the upper limit of integration were made. The width of the Lorentzian, A, is related to the dipolar broadening of the NMR signal by $\sigma = 3\omega_\mathrm{q}A$. After the integration [14] is done, the resulting analytic function is defined over all values of ω (thus R) and is written

$$\begin{aligned} f_\varepsilon(R,A,\eta,\phi) = \frac{1}{2\pi\varrho}\Bigg\{ & 2\cos(\alpha/2)\left[\arctan\left(\frac{Y^2-\varrho^2}{2Y\varrho\sin(\alpha/2)}\right)+\frac{\pi}{2}\right] \\ & +\sin(\alpha/2)\ln\left(\frac{Y^2+\varrho^2+2Y\varrho\cos(\alpha/2)}{Y^2+\varrho^2-2Y\varrho\cos(\alpha/2)}\right)\Bigg\}, \end{aligned} \tag{14}$$

where $\varrho^2=\sqrt{A^2+[1-\varepsilon R-\eta\cos(2\phi)]^2}$, $\cos(\alpha)=[1-\varepsilon R-\eta\cos(2\phi)]/\varrho^2$. Fig. 3 shows examples of the dipole broadened function of Eq. (14) compared to the simple function in Eq. (12) both with $\eta=0$. The two maxima of the dipole broadened function lie inside the pole positions which are at $R=\pm 1$. Thus, measuring the distance between the maxima of an NMR signal under-estimates the value of ω_q.

In order to use the function f_ε for fitting to deuteron NMR signals, first the dependence on the azimuthal angle ϕ will have to be averaged. This can be done numerically with the integral

$$F_\varepsilon(R,A,\eta) = \frac{2}{\pi}\int_0^{\pi/2} \frac{\sqrt{3}f_\varepsilon(R,A,\eta,\phi)}{\sqrt{3-\eta\cos(2\phi)}}\,\mathrm{d}\phi \approx \frac{1}{J+1}\sum_{j=0}^{J} \frac{\sqrt{3}f_\varepsilon(R,A,\eta,\phi_j)}{\sqrt{3-\eta\cos(2\phi_j)}}, \tag{15}$$

where $J=64$ is sufficient with ϕ_j evenly distributed over the $0\le\phi\le\pi/2$ range. Fig. 4 compares the function F_+ for the values $\eta=0$ and $\eta=0.16$ whose maximum occurs at $R=(1-\eta)$. The ratio of the peak width to the shoulder width is $\frac{1}{2}(1-\eta)$ which can be used to verify quickly whether $\eta>0$ or not when looking at an NMR signal.

In addition, any fitting algorithm has to evaluate the derivatives of the model function with respect to the fit parameters at each iteration. For the fitting to be efficient, the derivatives should be calculated analytically. For example, to fit an NMR signal, at each iteration the quantities

$$f_\pm\,,\quad \frac{\partial f_\pm}{\partial A}\,,\quad \frac{\partial f_\pm}{\partial\omega_\mathrm{q}}\,,\quad \frac{\partial f_\pm}{\partial\omega_0}\,,\quad \frac{\partial f_\pm}{\partial\eta}$$

will need to be evaluated, and then ϕ-averaged. It is easier to take derivatives of the simple function given in Eq. (12) and then do the convolution with the Lorentzian function than to take the derivatives of the function in Eq. (14). The necessary derivatives are explicitly written out in the appendix in terms of solutions to the convolution integrals.

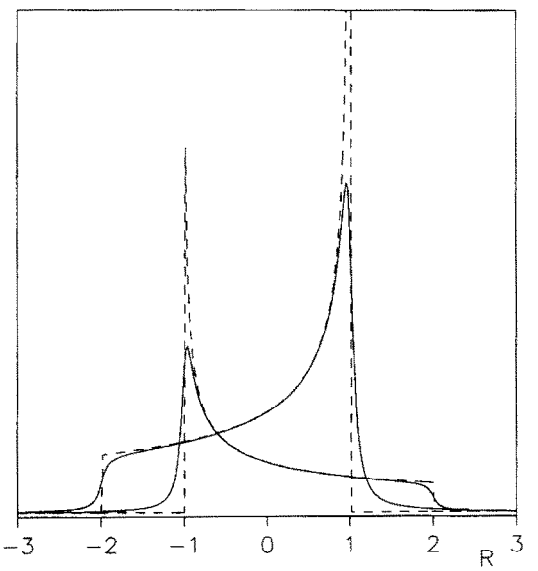

Fig. 3. Examples of absorption functions. The dashed lines are the naive line shape $(1 - \varepsilon R)^{-1/2}$ and the solid lines are the dipolar broadened functions of Eq. (14) evaluated with $\eta = 0$. The intensity factors are taken to be constants with the positive one being twice as large as the negative one.

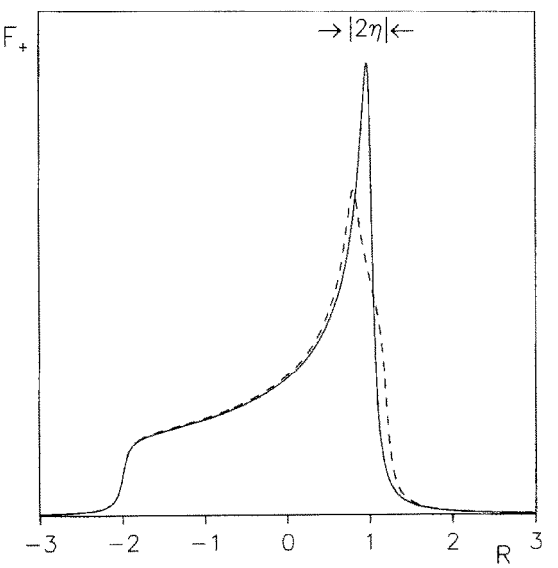

Fig. 4. A comparison of the line shapes for symmetric and asymmetric quadrupolar coupling. The solid line is the function F_+ calculated with Eq. (14) setting $\eta = 0$ while the dashed line is the ϕ-averaged function of Eq. (15) using $\eta = 0.16$.

2.1. Intensity factors

The absorption function $\chi''(\omega)$ is constructed by multiplying the polarization independent $F_\varepsilon(\omega)$ functions by the intensity factors which account for the dependence of the shape and size of the signal on polarization. The Boltzmann factor of the mth energy level is $n_m \sim e^{-\beta E_m}$. The differential populations of the three levels

of a spin-1 system are

$$\begin{aligned} \mathrm{d}n_+ &= \mathcal{N} \mathrm{e}^{\beta\hbar\omega_\mathrm{d} - \beta\hbar\omega_\mathrm{q}\lambda(\theta)}\, \mathrm{d}(\cos\theta), \\ \mathrm{d}n_- &= \mathcal{N} \mathrm{e}^{-\beta\hbar\omega_\mathrm{d} - \beta\hbar\omega_\mathrm{q}\lambda(\theta)}\, \mathrm{d}(\cos\theta), \\ \mathrm{d}n_0 &= \mathcal{N} \mathrm{e}^{2\beta\hbar\omega_\mathrm{q}\lambda(\theta)}\, \mathrm{d}(\cos\theta), \end{aligned} \tag{16}$$

where $\lambda(\theta) = \{[3 - \eta\cos(2\phi)]\cos^2(\theta) - [1 - \eta\cos(2\phi)]\}$, $\mathcal{N}$ is a normalization constant, and $\beta = (kT_s)^{-1}$ with T_s being the spin temperature of the system. Integrating over the angle θ and averaging over the angle ϕ yields the level populations

$$\begin{aligned} n_+ &\approx \mathcal{N} \mathrm{e}^{\beta\hbar\omega_\mathrm{d}} \{1 + \tfrac{2}{5}(\beta\hbar\omega_\mathrm{q})^2\}, \\ n_- &\approx \mathcal{N} \mathrm{e}^{-\beta\hbar\omega_\mathrm{d}} \{1 + \tfrac{2}{5}(\beta\hbar\omega_\mathrm{q})^2\}, \\ n_0 &\approx \mathcal{N} \{1 + \tfrac{8}{5}(\beta\hbar\omega_\mathrm{q})^2\}, \end{aligned} \tag{17}$$

from which the polarization of the spin system is to be calculated as

$$P = \frac{n_+ - n_-}{n_+ + n_- + n_0} = \frac{(n_+/n_-) - 1}{(n_+/n_-) + (n_0/n_-) + 1}. \tag{18}$$

These equations can be rewritten in terms of a parameter called the asymmetry, which will be defined here to be $r = \mathrm{e}^{\beta\hbar\omega_\mathrm{d}}$ so that it depends only on the polarization (through T_s) and not in any way on the frequency of the irradiating RF field. Investigating the ratios of the Boltzmann factors from the above equations, it is seen that

$$\frac{n_+}{n_-} = r^2 \qquad \text{and} \qquad \frac{n_0}{n_-} \approx r[1 + \tfrac{6}{5}(\beta\hbar\omega_\mathrm{q})^2] \tag{19}$$

and therefore that there is no correction to the polarization to first order in $\beta\hbar\omega_\mathrm{q}$. In terms of the asymmetry parameter, the polarization reads

$$P_\mathrm{AS} = \frac{r^2 - 1}{r^2 + 1 + r} + \mathcal{O}((\beta\hbar\omega_\mathrm{q})^2)\,. \tag{20}$$

The asymmetry r is a good parameter to use for determining polarization only if it can be related to the line shape, and this is done through the intensity factors. The intensity factors of Eq. (12) can be written

$$\frac{\mathrm{d}I_+}{\mathrm{d}(\cos\theta_+)} = C\frac{(\mathrm{d}n_+ - \mathrm{d}n_0)}{\mathrm{d}(\cos\theta_+)} \sim \frac{r^2 - r^{1+3\vartheta\lambda(\theta)}}{r^{1+\vartheta\lambda(\theta)}} = \frac{r^2 - r^{1-3\vartheta R}}{r^{1-\vartheta R}} \tag{21}$$

and

$$\frac{\mathrm{d}I_-}{\mathrm{d}(\cos\theta_-)} = C\frac{(\mathrm{d}n_0 - \mathrm{d}n_-)}{\mathrm{d}(\cos\theta_-)} \sim \frac{r^{1+3\vartheta\lambda(\theta)} - 1}{r^{1+\vartheta\lambda(\theta)}} = \frac{r^{1+3\vartheta R} - 1}{r^{1+\vartheta R}}, \tag{22}$$

where $\vartheta = \omega_\mathrm{q}/\omega_\mathrm{d}$ is the strength of the quadrupole splitting compared to the Zeeman splitting and the relation $-\varepsilon R = \lambda(\theta)$ was used to replace the λ-function. Remember, the $\varepsilon = \pm 1$ sign goes with the subscript on I_ε, the intensities, not with the subscript on n_m, the populations.

When the quadrupolar coupling is weak ($\vartheta \ll 1$), as in the case for the deuteron signals taken at 2.5 T for which $\omega_\mathrm{d} = 2\pi \times 16.35\,\mathrm{MHz}$, the intensity factors are in good approximation independent of the frequency for a given polarization and they have a ratio

$$\frac{\mathrm{d}I_+/\mathrm{d}(\cos\theta_+)}{\mathrm{d}I_-/\mathrm{d}(\cos\theta_-)} \approx r^{1-\vartheta R} \approx r\,. \tag{23}$$

Therefore, a fitting function of the form $\chi'' \propto rF_+ + F_-$ can be used to fit deuteron NMR signals, which shows why r is called the asymmetry parameter. In order to estimate the polarization, one only needs to

measure the heights of the peaks. Then, the ratio of the heights is the asymmetry, r, from which Eq. (20) is used to determine the polarization. This works for deuterated butanol because $\vartheta \approx 10^{-3}$ in a 2.5 T field. However, in the case of a nitrogen-14 nucleus in an ammonia molecule, the value is $\vartheta \approx 0.06$ in a 2.5 T field and therefore the intensity factor ratio would neither indicate the asymmetry, nor the polarization, because it would vary greatly across the measured frequency range. With $\vartheta = 10^{-3}$ the variation of the intensity factors in Eqs. (21) and (22) across the range $R = \pm 2$ is about 1% whereas with $\vartheta = 0.06$ the variation is 50% or so. Therefore, for nitrogen signals in ammonia, the dependence of the intensity factors will be an important component of the line shape [18].

The correct way to determine the asymmetry, r, is by fitting the equation of the absorption function from this theory to NMR signals, not by dividing the peak heights. Then the polarization can be calculated from Eq. (20). Using Eqs. (14, 15, 21, 22) the absorption function for large quadrupole broadening reads

$$\chi''(r,R) \propto \left(\frac{1}{\omega_q}\right)\left\{\left[\frac{r^2 - r^{1-3\vartheta R}}{r^{1-\vartheta R}}\right] F_+(R) + \left[\frac{r^{1+3\vartheta R} - 1}{r^{1+\vartheta R}}\right] F_-(R)\right\}, \tag{24}$$

while for deuterated butanol material in a 2.5 T field, where $\vartheta \gg 1$, the absorption function in good approximation is

$$\chi''(r,R) \propto \left(\frac{1}{\omega_q}\right)\left(\frac{r-1}{r}\right)[rF_+(R) + F_-(R)]. \tag{25}$$

However, the absorption function for deuterated butanol includes contributions from both the C–D and O–D bonds where the quadrupolar coupling ω_q (thus R) differs between the bonds. The dipolar broadening parameter $\sigma = 3\omega_q A$ should be the same for the two bonds, whereas A will be different. It is assumed that the polarization of the deuterons is the same whether they are attached to carbon or oxygen. The experimental deuteron signals of Figs. 6 and 7 show that $\eta = 0$ for the C–D bond since the shoulder width is twice as large as the peak width. Moreover, a constant factor K representing the relative amount of O–D to C–D bonds should multiply the contribution from the O–D bonds. The constant will contain a contribution from the 5% by weight of heavy water that is used so that the material does not crystalize during production [15]. Therefore, the NMR signal should have contributions of roughly 85.5% from the C–D bonds, 9.5% from the O–D bonds of butanol and another 5% from the O–D bonds in the heavy water. A value $K = 0.136$ is expected after accounting for the relative densities of the butanol and heavy water. To wit, the total absorption function for butanol is

$$\chi''_{\text{but}}(r,R,\sigma,\eta) = (1-K)\chi''(r,\sigma,R^{\text{car}},\eta = 0) + K\chi''(r,\sigma,R^{\text{oxy}},\eta)\ , \tag{26}$$

where either of Eqs. (24) or (25) can be used to represent χ'' for analyzing deuteron signals. Fig. 5 shows an example of how the contributions from the four F's could combine to make up an absorption function.

3. Q-meter corrections

Before the expression for χ''_{but} in Eq. (26) can be employed, it is necessary to make corrections for errors arising from the NMR system itself. One error pertains to the distortion of the signal of χ'' caused by the Q-meter and the other is for time dependencies of the properties of the Q-meter.

3.1. Residual background

Earlier it was assumed in the relation $S(\omega) = \text{Re}\{V(\omega,\chi) - V(\omega,0)\} \propto \chi''(\omega)$ that the properties of the Q-meter do not change between the times when the Q-curve $V(\omega,0)$ and the signal $V(\omega,\chi)$ are taken. This is not entirely true; there is a time dependence that causes a "residual background" in the subtracted signal $S(\omega)$. Since the subtraction of two Q-curves taken at different times can be considered a third-order polynomial in all but the worst cases [16], the residual background can be removed by fitting a polynomial of third order

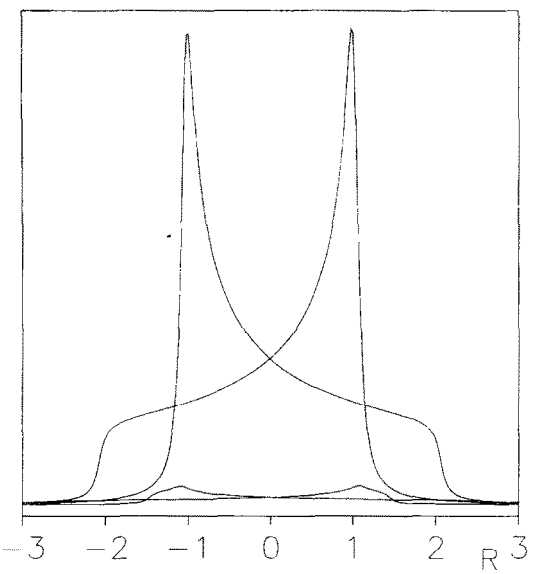

Fig. 5. Example of the C–D and O–D bond contributions to an absorption function. The C–D bond peaks are the taller ones occurring at $R = \pm 1$ and the O–D bond peaks are the shorter wider peaks. The C–D lines are calculated with $\eta = 0$ and the O–D lines with $\eta = 0.15$.

to the wings of the NMR signal, where the absorption function is sufficiently close to zero. However, this procedure will force the wings to be flat, where in fact, there should be small tails from the dipolar broadening. Therefore, in this analysis the background will be included in the description of the signal. Then the signal model, including the background, will be fit simultaneously to all data points of the NMR signal. To this end, the working definition of the experimental NMR signal as the sum of the absorption function and the residual background reads

$$S(\omega) \propto \chi''_{\text{but}}(\omega) + a_0 + a_1\omega + a_2\omega^2 + a_3\omega^3, \tag{27}$$

where a third-order polynomial in ω representing the residual background is included. An additional complication is that the NMR system itself also causes distortions which need to be corrected before a reliable signal line-shape analysis can be done.

3.2. *False asymmetry and false polarization*

The Q-meter distortions appear as a false asymmetry in the deuteron TE signal. It manifests itself by increasing the size of the right side of the signal by a few percent with respect to the left side. Since the TE signal has a small and well-known asymmetry which results from its $P_{\text{TE}} = 0.0523\,\%$ polarization, it provides a very clean way to measure this asymmetry and therefore it enables the parameterization of the effects of the Q-meter distortions.

A more exact relation [17] for Eq. (3) is available and can be used to estimate higher-order frequency-dependent corrections to the NMR signal defined in Eq. (27). A detailed example calculation of this distortion can be found in Ref. [18] which shows that a small mixing of χ' into the signal causes this effect. The distortion is approximated well be a linear gain across the deuteron signal which can be summarized by

$$D(\omega) = 1 + \tfrac{1}{2}\xi(1 + R), \tag{28}$$

where ξ is the false asymmetry parameter. The equation is written in this manner so that ξ is directly the difference in gain between the two peaks of the signal. Now, the false asymmetry correction to χ'' is put

together with the residual background correction, and the result is the NMR signal. In summary, the NMR signal from the Q-meter is

$$S(\omega) = \mathcal{Q}\,\chi''_{\text{but}}(\omega)[1 + \tfrac{1}{2}\xi(1+R)] + a_0 + a_1\omega + a_2\omega^2 + a_3\omega^3 \tag{29}$$

where $\mathcal{Q}$ is used to represent the constant gain factors of the Q-meter as well as the physical constants.

4. Results of the signal analysis

The full theoretical expression for the NMR signal that is fit to the data is found by looking back through Eqs. (29), (26), (24), (15), (14), amongst which there are a total of 13 fitting parameters. The absorption function is described by the eight parameters $\mathcal{Q}$, r, ω_d, σ, ω_q^{car}, ω_q^{oxy}, plus η for the O–D bond only, and K from the mixing of O–D and C–D contributions. In addition, the instrumentation requires 5 fitting parameters: ξ, from the false asymmetry, and a_0 to a_3, from the residual background. For this analysis, the absorption function of Eq. (24) which includes frequency-dependent intensity factors was used.

The NMR signals consist of 200 sweeps at enhanced polarizations and 2000 sweeps at TE polarizations. The Q-meter voltage is sampled at 400 evenly spaced frequencies (every 1.25 kHz) along the sweep range between 16.1–16.6 MHz. All 400 data points are used to fit the signals. For enhanced signals, the noise is sufficiently reduced to permit fitting after averaging over 200 double sweeps. However, the fitting for TE signals requires that many TE signals of 2000 double sweeps be averaged to make a super-TE-signal before the signal-to-noise ratio is sufficient to allow accurate fitting.

In the SMC polarized target [4], there were nine NMR coils measuring the polarization in parallel during the 1995 data taking. For the analysis presented below, the results and plots were made using signals from one coil only. However, the results obtained from the other coils were also analyzed on a smaller data sample and agreed for all the coils.

4.1. Polarization

The first step in the analysis is to determine the asymmetry parameter ξ from the TE signals, for which the polarization is known and thus the asymmetry also. For example, at $P_{TE} = 0.0523\%$ the asymmetry is $r = 1.0008$. However, when the model is fit to the super-TE-signal with $\xi = 0$, a false polarization of $P_{AS} = 3.81\%$ and an asymmetry of $r = 1.059$ are found. Fortunately, there is a way to find the value of ξ. Fitting $S(\omega)$ to a super-TE-signal with the asymmetry fixed to $r = 1.0008$ and ξ allowed as a free parameter yields a value of $\xi = 0.048$, which Fig. 6 demonstrates. Because the false asymmetry $r = 1.059$ is close to the sum $1.0008 + 0.048$, it is assumed that the linear approximation to $D(\omega)$ given in Eq. (28) is sufficient to take into account all effects arising from the Q-meter, including distortions multiplying χ'' and any dispersion contributions.

As a side note, the value $\xi = 0.048$ applies only if the intensity factors are taken as frequency dependent. However, if the frequency dependence of the intensity factors is ignored and Eq. (25) is used instead of Eq. (24), a value $\xi = 0.057$ is obtained. Thus, even with a perfect detection system, the peak heights for deuterons with TE polarizations at 1 K should not be equal, but the right peak should be 1% taller than the left one.

Now, the parameter $\xi = 0.048$ is known and can be kept constant at all polarizations. With the ξ correction, the agreement between polarizations calculated with the two methods is excellent. Fig. 7 shows a fit to an enhanced signal where the results are $P_{AR} = 44.27\%$ from the area method and $P_{AS} = 44.80\%$ from the asymmetry method.

An in-depth study of the polarizations calculated with the two methods results in Fig. 8 where P_{AS} is plotted versus P_{AR} for both signs of polarization as the polarization grows at the maximum possible rate during the DNP process. For polarizations above 30%, the agreement between the two methods is within the $\pm 3.0\%$ relative error of the TE-calibrated method. The determination of the polarization from the asymmetry method

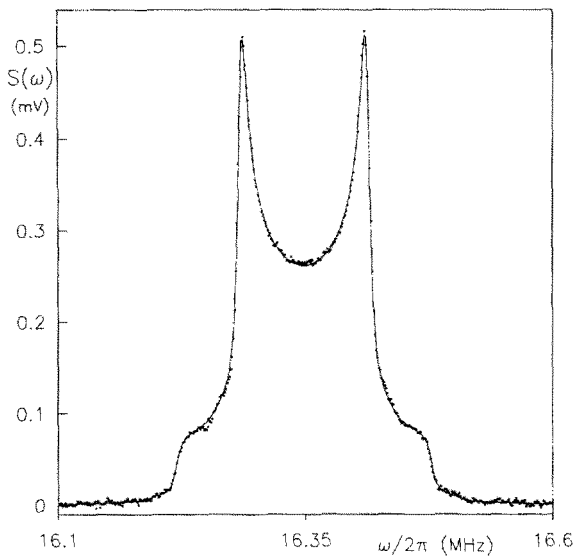

Fig. 6. The super-TE-signal (circles) with the fitted curve superimposed (line).

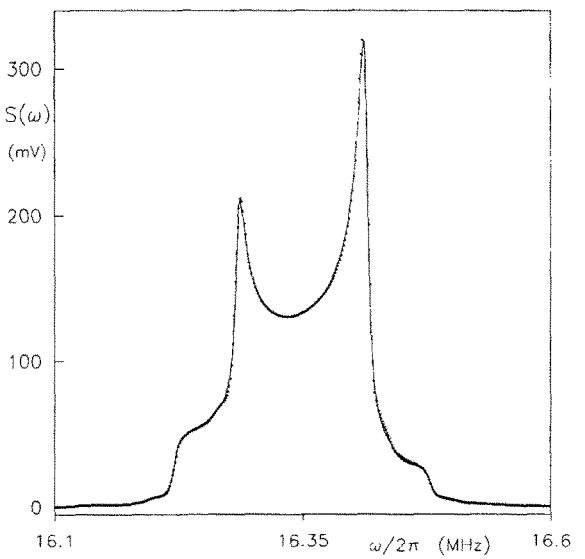

Fig. 7. An enhanced signal of 44% polarization (circles) with the fitted curve superimposed (line).

assumes the polarization is uniform throughout the sampling range of the coil since one temperature T_s (i.e. β) is used to describe the system. The good agreement between the two methods at the highest polarizations supports the spin temperature theory and implies that the polarization is homogeneous throughout the sampling range of the coil. At the lower polarizations the two methods diverge slightly which is an indication that at these values the polarization is not uniform due to the DNP process.

The dominant error of the asymmetry method is the 1.0% absolute error occurring when ξ and r are allowed as free parameters. However, if the correction for the false asymmetry is made this error will be smaller. The total error is about 3.0% accounting for the uncertainties in fitting ξ and the removal of the residual background.

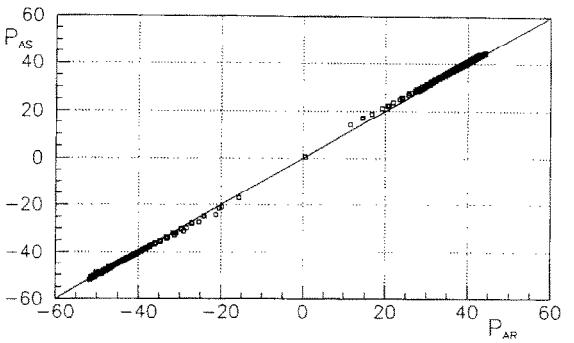

Fig. 8. A plot of P_{AS} versus P_{AR} with the $P_{AS} = P_{AR}$ line superimposed. This data represents signals taken at different times over the span of several months. The deviation at lower polarizations may be a sign of non-uniform polarization occurring during the DNP process.

4.2. Fitting parameters and properties of butanol

From the theory of the deuteron line shape and the fitting procedure outlined above, some properties of deuterated butanol can be measured. The quadrupolar coupling constant (ω_q) and dipolar broadening ($\sigma = 3\omega_q A$) for both the C–D and O–D bonds are parameters of the fitting paradigm. The following properties were determined by fitting the theoretical line shape to enhanced signals

$\omega_q^{car}/2\pi = 21.58 \pm 0.04\,\text{kHz}$ or $\text{eq}\,eQ/h = 172.6 \pm 0.3\,\text{kHz}$,

$\omega_q^{oxy}/2\pi = 26.6 \pm 0.1\,\text{kHz}$ or $\text{eq}\,eQ/h = 213 \pm 1\,\text{kHz}$,

$\sigma/2\pi = 4.0 \pm 0.1\,\text{kHz}$,

$$\frac{\omega_q^{oxy}}{\omega_q^{car}} = 1.23 \pm 0.01,$$

$\eta = 0.15 \pm 0.01$ (oxygen bond only),

$K = 0.065 \pm 0.015$.

The errors on the numbers are the statistical errors coming from the average of the 490 enhanced polarization signals that were used to make Fig. 8 and which were taken at various times during several months of operation. The false asymmetry correction introduces no error in the measurements of these constants since the values of the ω_q's and σ when $\xi = 0$ agreed with those when $\xi = 0.048$ to well within the statistical errors quoted above. However, the statistical errors on the determinations with $\xi = 0$ were a few percent larger than those with the correction. If ξ is left free for the fitting of the signals, the averages and errors are the same as if $\xi = 0.048$ were used for all signals. In addition, there were small signal-by-signal differences in the values of the parameters above. The average value of the false asymmetry parameter was $\xi = 4.5 \pm 0.9$ when it was left free.

Similar methods have been used in previous works by Hamada et al. [20] and Wait et al. [21] to fit theoretical line shapes to deuteron signals in hydro-carbon materials, and their determinations of the parameters ω_q^{car}, ω_q^{oxy}, σ and η are consistent with our results. However, these analyses assumed the value of K depending on the chemical composition of their target materials.

The constant $K = 0.065$, which represents the amount of signal coming from the O–D bonds relative to the C–D bonds, is about a factor of two smaller than the expectation of $K = 0.136$ based on the chemical composition of the target material consisting of deuterated butanol with 5% by weight of heavy water. The contribution to the integrated NMR signals from the C–D bonds is proportional to $(1-K)$, or $P(\text{C–D}) \propto (1-K)$, while the contribution from the O–D bonds is proportional to K, or $P(\text{O–D}) \propto K$. It is possible to use two

separate asymmetry parameters to describe the NMR signal: one for the C–D bond and another for the O–D bond. If this is done, then it is found that $P_{AS}(O-D)= (0.7 \pm 0.3)P_{AS}(C-D)$. If this is a real effect, it may be due to either a lower deuteron polarization in the O–D bonds of water, or a lower polarization of the deuterons in the O–D bonds relative to those in the C–D bonds.

5. Conclusions

An analytical model of the spin-1 line shape has been developed which includes dipolar broadening, frequency dependence of the intensity factors, and corrections for Q-meter effects. When used to analyze deuteron NMR signals, it gives polarization values consistent with the standard area method to within the 3% errors of the two methods. Consideration of the frequency dependence of the intensity factors has a small but noticeable effect for deuteron signals. In contrast, for materials such as nitrogen nuclei in ammonia where the quadrupole splitting is much stronger compared to the Zeeman splitting than in deuterated materials, the frequency dependence of the intensity factors will be important for determining polarization from such signals.

The asymmetry method as used in this article is not meant as a substitution for a good TE calibration as a method for determining the polarization. A good measurement of the area of the TE signals is needed for calibrating the NMR system in the area method while a measurement of the TE line shape is helpful for adjusting ξ in the asymmetry method. The asymmetry method allows confirmation of the polarization values and tells whether the polarization throughout the sampling range of the coil is homogeneous.

If needed, the asymmetry method could be used with a limited accuracy in cases where no TE-calibration is possible. For example, it could be used in very small samples of materials where there simply are not enough spins to see a signal under TE conditions. In this case, the false asymmetry parameter can be left free and an accuracy of 5% is within reach.

Finally, the magnitude of the quadrupolar coupling constant and the dipolar broadening of the C–D to O–D bonds in deuterated butanol have been determined. The values of these constants are the same whether or not the correction for the false asymmetry is made, and agree with similar measurements done before.

Appendix A.

In fitting methods used for nonlinear equations such as the model function for the absorption of Eq. (25) used in this paper, not only is it necessary to evaluate the function at each iteration, but it is also necessary to evaluate the derivatives with respect to the fitting parameters. For example, in the fitting discussed in this paper, the function f_ε and its derivatives $\partial f_\varepsilon/\partial\omega_d$, $\partial f_\varepsilon/\partial A$, and $\partial f_\varepsilon/\partial\eta$ need to be evaluated in order to fit the model function to the NMR signals. Instead of trying to take derivatives of equations such as Eq. (14), it is easier to exchange the order of integration and differentiation. That is, first take the derivative of Eq. (13), then integrate the resulting equation.

Let us start the calculation of the derivatives by defining the function that appears in the integrand of Eq. (13), namely,

$$g(y) = y^4 - 2zy^2 + A^2 + z^2, \tag{A.1}$$

where $z = [1 - \varepsilon R - \eta\cos(2\phi)]$, and then also the two functions that appear in Eq. (14), namely,

$$L = \frac{1}{2}\ln\left(\frac{y^2+\varrho^2+2y\varrho\cos(\alpha/2)}{y^2+\varrho^2-2y\varrho\cos(\alpha/2)}\right) \quad \text{and} \quad T = \arctan\left(\frac{y^2-\varrho^2}{2y\varrho\sin(\alpha/2)}\right). \tag{A.2}$$

The integral appearing in Eq. (13) can be written and evaluated in terms of these functions, resulting in [14]

$$\mathcal{I}_1 = \int_0^Y \frac{dy}{g(y)} = \frac{1}{2\varrho A}\left[\left(T+\frac{\pi}{2}\right)\cos(\alpha/2) + L\sin(\alpha/2)\right]. \tag{A.3}$$

For calculating the necessary derivatives, recursion relations can be used. However, for the recursion relations, another integral whose solution is not in Ref. [14] needs to be evaluated first. This integral is

$$\mathscr{I}_2 = \int_0^Y \frac{y^2 \mathrm{d}y}{g(y)} = \frac{\varrho}{2A}\left[T\cos(\alpha/2) - L\sin(\alpha/2)\right]. \tag{A.4}$$

The density of states function is $f_\varepsilon = (2A/\pi)\mathscr{I}_1$ and the derivatives with respect to R and A in terms of convolution integrals are

$$\frac{\partial f_\varepsilon}{\partial A} = \frac{2A}{\pi}\frac{\partial \mathscr{I}_1}{\partial A} = \frac{2}{\pi}\mathscr{I}_1 - \frac{4A^2}{\pi}\int_0^Y \frac{\mathrm{d}y}{g^2(y)} \equiv \frac{2}{\pi}[\mathscr{I}_1 - 2A^2\mathscr{I}_3] \tag{A.5}$$

and

$$\frac{\partial f_\varepsilon}{\partial R} = \frac{2A}{\pi}\left\{2\varepsilon z\int_0^Y \frac{\mathrm{d}y}{g^2(y)} - 2\varepsilon\int_0^Y \frac{y^2\mathrm{d}y}{g^2(y)}\right\} \equiv \frac{4A\varepsilon}{\pi}\{z\mathscr{I}_3 - \mathscr{I}_4\}. \tag{A.6}$$

Now, the integrals $\mathscr{I}_3$ and $\mathscr{I}_4$ required for evaluating the derivatives in the last two equations can be solved with recursion relations involving $\mathscr{I}_1$ and $\mathscr{I}_2$, which are [14]

$$\mathscr{I}_3 = \frac{1}{4A^2\varrho^2}\left\{\frac{Y}{g(Y)}[Y^2 z + 2A^2 - \varrho^4] + (2A^2 + \varrho^4)\mathscr{I}_1 + z\mathscr{I}_2\right\} \tag{A.7}$$

and

$$\mathscr{I}_4 = \frac{1}{4A^2}\left\{\frac{Y}{g(Y)}[Y^2 - z^2] + z\mathscr{I}_1 + \mathscr{I}_2\right\}. \tag{A.8}$$

The last derivative to calculate is $\partial f_\varepsilon/\partial\eta$, which, using a relation found in Ref. [19], is

$$\frac{\partial f_\varepsilon}{\partial\eta} = \frac{\partial}{\partial\eta}\int_0^{Y(\eta)} \frac{\mathrm{d}y}{g(y,\eta)} = \int_0^Y \frac{\partial}{\partial\eta}\left(\frac{1}{g(y,\eta)}\right)\mathrm{d}y + \frac{1}{g(Y,\eta)}\frac{\mathrm{d}Y}{\mathrm{d}\eta} \tag{A.9}$$

and, therefore, after evaluation yields

$$\frac{\partial f_\varepsilon}{\partial\eta} = \frac{4A\cos(2\phi)}{\pi}\left\{z\mathscr{I}_3 - \mathscr{I}_4 - \frac{1}{4Yg(Y)}\right\}. \tag{A.10}$$

Now, the derivatives with respect to f_ε can be averaged over ϕ and then combined to get derivatives with respect to $\chi''(\omega)$ in the same manner as Eq. (26) was constructed from the f_ε functions.

References

[1] M. Goldman, J. Magn. Res. 17 (1975) 393.
[2] A. Abragam, Principles of Nuclear Magnetism, Clarendon Press, Oxford, 1961, p. 75.
[3] G.R. Court et al., Nucl. Instr. and Meth. A 324 (1993) 433.
[4] B. Adeva et al., Nucl. Instr. and Meth. A 349 (1994) 334.
[5] N. Hayashi et al., Nucl. Instr. and Meth. A 356 (1995) 91.
[6] A. Abragam, Principles of Nuclear Magnetism, Clarendon Press, Oxford, 1961, pp. 392, 401.
[7] B. Adeva et al., Nucl. Instr. and Meth. A 372 (1996) 339.
[8] J.D. Jackson, Classical Electrodynamics, Wiley, New York, 1975, p. 142.
[9] A. Abragam, Principles of Nuclear Magnetism, Clarendon Press, Oxford, 1961, pp. 217, 236.
[10] W. de Boer, Dynamic Orientation of Nuclei at Low Temperatures, CERN Yellow Report 74-11 (1974).
[11] W. Kielhorn, Los Alamos Report LA-12116-T (1991).
[12] M.H. Cohen, F. Reif, Nuclear quadrupole effects in solids, in: Solid State Physics, vol. 5, Academic Press Inc., New York, 1957.
[13] A. Abragam, Principles of Nuclear Magnetism, Clarendon Press, Oxford, 1961, pp. 159, 166.
[14] I.S. Gradshteyn, I.M. Ryzhic, Table of Integrals, Series, and Products, Corrected and Enlarged edition, Academic Press Inc., New York, 1980, p. 67.

[15] S. Bültmann et al., Nucl. Instr. and Meth. A 356 (1995) 102.
[16] C.M. Dulya, Nucl. Instr. and Meth. A 356 (1995) 88.
[17] Yu.F. Kisselev, C.M. Dulya, T.O. Niinikoski, Nucl. Instr. and Meth. A 354 (1995) 249.
[18] C.M. Dulya, Ph.D. Thesis, University of California, Los Angeles, CA, 90095, USA, 1996.
[19] W.H. Beyer (ed.), CRC Standard Math Tables, 28th edn., CRC Press Inc., Boca Raton, FL, USA, 1987, p. 232.
[20] O. Hamada et al., Nucl. Instr. and Meth. 189 (1981) 561.
[21] G.D. Wait et al., Nucl. Instr. and Meth. A 274 (1989) 515.